PROCEEDINGS OF SCIENCE

Multidimensional simulations of core-collapse supernovae and implications for nucleosynthesis

W. Raphael Hix[ab], J. Austin Harris[b], Eric J. Lentz[b], Stephen Bruenn[c], Austin Chertkow[b], O.E. Bronson Messer[da], Anthony Mezzacappa[be], John Blondin[f], Eirik Endeve [g],Pedro Marronetti[h], and Konstantin N. Yakunin[b] *

[a] *Physics Division, Oak Ridge National Laboratory, Oak Ridge TN 37831-6354 USA*
[b] *Department of Physics and Astronomy, University of Tennessee, Knoxville, TN 37996-1200 USA*
[c] *Department of Physics, Florida Atlantic University, Boca Raton, FL 33431-0991 USA*
[d] *National Center for Computational Sciences, Oak Ridge National Laboratory Oak Ridge TN 37831-6008 USA*
[e] *Joint Institute for Computational Sciences, Oak Ridge National Laboratory Oak Ridge TN 37831-6173 USA*
[f] *Department of Physics, North Carolina State University, Raleigh, NC 27695-8202 USA*
[g] *Computer Science & Mathematics Division, Oak Ridge National Laboratory Oak Ridge TN 37831-6164 USA*
[h] *Physics Division, National Science Foundation, Arlington, VA 22207 USA*

Core-collapse supernovae (CCSNe), the culmination of massive stellar evolution, are the principle actors in the story of our elemental origins. Our understanding of these events, while still incomplete, centers around a neutrino-driven central engine which is highly hydrodynamically-unstable. Simulations of increasing sophistication show a shock that stalls for hundreds of milliseconds before reviving. Though brought back to life by neutrino heating, the development of the supernova explosion is inextricably linked to three dimensional fluid flows. Regrettably, much of our understanding of the nucleosynthesis that occurs in these explosions, and their impact on galactic chemical evolution, is based on spherically symmetric simulations with parameterized explosions, ignoring much that has been learned about the central engine of these supernovae over the past two decades. Here we discuss recent results from two-dimensional CCSN simulations using our CHIMERA code, as well as ongoing three-dimensional simulations, and discuss how the multidimensional character of the explosions directly impacts the nucleosynthesis and other observables of core-collapse supernovae.

XIII Nuclei in the Cosmos
7-11 July, 2014
Debrecen, Hungary

*This work supported by grants from the NASA Astrophysics Theory Program (NNH11AQ72I), by the National Science Foundation PetaApps Program (grants OCI-0749242, OCI-0749204, and OCI-0749248) and by the Department of Energy Offices of Nuclear Physics and Advanced Scientific Computing Research. Computational resources provide by NSF TeraGrid at the National Institute for Computational Sciences (grant number TG-MCA08X010) and by DoE Office of Science through the National Energy Research Scientific Computing Center (Contract No. DE-AC02-05CH11231) and the INCITE program at the Oak Ridge Leadership Computing Facility (Contract No. DE-AC05-00OR22725). PM is supported by the National Science Foundation through its employee IR/D program. The opinions and conclusions expressed herein are those of the authors and do not represent the National Science Foundation.

PoS(NIC XIII)019

1. Introduction

Beyond their spectacular visible display as core-collapse supernovae (CCSNe), the deaths of massive stars ($M \gtrsim 8\,M_{\odot}$) are the dominant source of elements in the periodic table between oxygen and iron as well as marking the formation of a neutron star (NS) or black hole. There is growing observational evidence that CCSNe, or one of the related deaths of massive stars, are linked to the production of half the elements heavier than iron in the r-process, although current simulations are hard–pressed to confirm this. Core collapse supernovae serve both to disperse elements synthesized within massive stars during their lifetimes and to synthesize and disperse new elements, providing an important link in our chain of origin from the Big Bang to the present. In the process, the ejecta of a supernova delivers 10^{51}ergs of kinetic energy, providing a major source of heat in the ISM as well as a potential trigger for star formation.

The challenges of modeling the central engine of these supernovae (the newly-formed neutron star, its neutrino radiation field and the region, perhaps 1000 km in radius, where these neutrinos deliver energy to power the explosion) has often left the modeling of the supernova's impact on the outer regions of the star, the circumstellar environment and Galactic chemical evolution to less sophisticated models. Much of our current understanding of nucleosynthesis in core-collapse supernovae is based on parameterized models which replace the central engine of the supernova with a kinetic energy *piston* or a thermal energy *bomb*, where the explosion's energy, its delay time and/or the *mass cut*, which separates the ejecta from matter destined to become part of the neutron star, are externally supplied parameters. Those models, unfortunately, ignore much that we have learned in the past two decades about the nature of these neutrino-driven, hydrodynamically-unstable explosions. However, bomb/piston models have the benefit that dozens of models, for stars with different masses, metallicities, rotation rates, etc., can be run at reasonable computational cost to provide input to investigations, e.g. Galactic Chemical Evolution, which depend on a multitude of dying stars. In the following sections, we will discuss recent progress in self-consistent modeling of the CCSN central engine, with an eye toward what this may teach us about supernova nucleosynthesis and the requirements to model this nucleosynthesis accurately.

2. Recent Progress in Two Dimensions

The physical complexity of the CCSN central engine places stringent requirements on simulations that seek to uncover its mysteries. While less costly approximations may be appropriate for some investigations, fundamental investigations of the CCSN mechanism will ultimately require three-dimensional simulations that include, among other things, general relativity, neutrino transport and detailed prescriptions of the microscopic properties of matter and the interactions between the neutrinos and matter. A number of investigations of these requirements can be found [see, e.g., 1, 2, and references therein]. These studies are extremely valuable but represent only half of the process by which computational simulations should be tested. Ultimately, the physical fidelity of simulations is tested by verification, comparison to known solutions (and in the case of complex problems, to other simulations) as well as by validation, comparison to experiment or observations.

Bruenn et al. [4, 3] have recently published a set of axisymmetric self-consistent models using the CHIMERA code for 12, 15, 20 and 25 $M_{\odot}$ progenitors from Woosley and Heger [5]. In

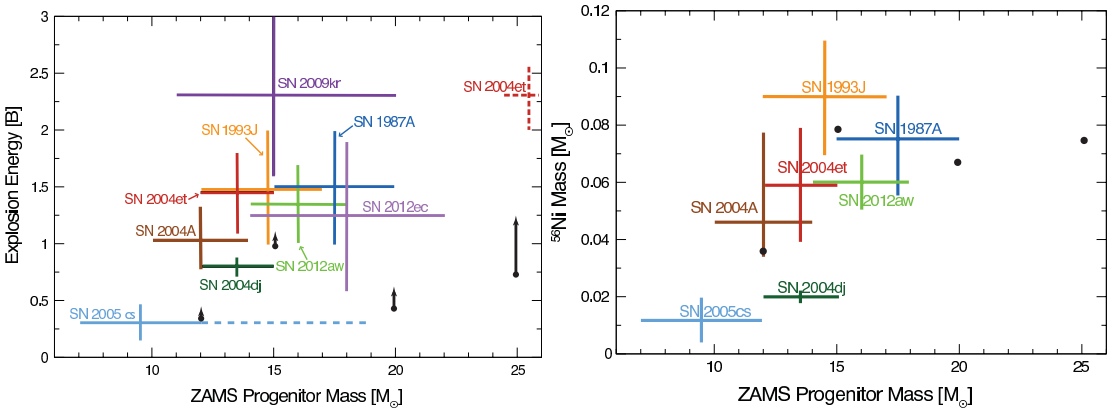

Figure 1: Comparison of the explosion energy and nickel mass determined from observations to those resulting from axisymmetric simulations from the CHIMERA code. See Bruenn et al. [3] for more details.

all 4 cases, robust explosions are exhibited, characterized by neutrino-driven outflows along each pole fed by an equatorial downflow that allows accretion to continue even after the explosion has commenced. The left panel of Figure 1 represents an initial attempt at validation for these models, comparing simulation results with observations of the explosion energy (kinetic energy of the ejecta). Because the explosions in these CHIMERA models are $\sim$ 1 second old, their internal energy dominates over the kinetic energy. Furthermore, the eventual ejecta remains deep in the star's gravitational well. Thus any estimate of the eventual explosion energy must sum the kinetic energy, internal (thermal) energy and (negative) gravitational energy, to reflect the conversion of internal energy to kinetic energy as the shock reaches the surface of the star and the need to lift the ejecta out of the star's gravity well. A common measure used in the literature is the *diagnostic energy*, the sum of this local total energy over all zones where this total is positive. To estimate the eventual explosion energy that will develop as the shock propagates to the surface of the star, the gravitational binding energy of the envelope above the shock must be subtracted from the diagnostic energy, reflecting the need for the shock to lift the entire envelope out of the star's gravitational potential. The values from the CHIMERA models are plotted as arrows, with the base as the value at the termination of each model and the length of the arrow reflecting the then current growth rate, in Bethe (10^{51} ergs) per sec. The general trend is that more massive progenitors produce more powerful explosions, with the exception of the 20 $M_\odot$ case, where the equatorial accretion flow was prematurely cut off by the lateral growth of the polar outflows. The observational values for individual supernovae are plotted as crosses, with the vertical and horizontal bars reflecting uncertainties in the explosion energy and progenitor mass. Bruenn et al. [3] details the sources for these data and the determination of the uncertainties. Additional systematic errors are possible, for example, inconsistencies between the stellar models used to determine progenitor mass from archival images [for example, 6, 7] and the progenitor models used in the CHIMERA simulations [5]. While such errors would likely make the uncertainties even larger, it is nevertheless important to make the attempt to constrain the models with observations to the extent this is possible. The CHIMERA models predict explosion energies comparable to, but somewhat smaller than, observations.

This relative success in achieving reasonable explosion energies motivates the comparison to additional observables. Because of the role ^{56}Ni plays in powering the visible supernova, determinations of the mass of ^{56}Ni ejected are a common observational constraint. The right panel of Figure 1 compares a set of these observational constraints to the results of the Bruenn et al. [3] mod-

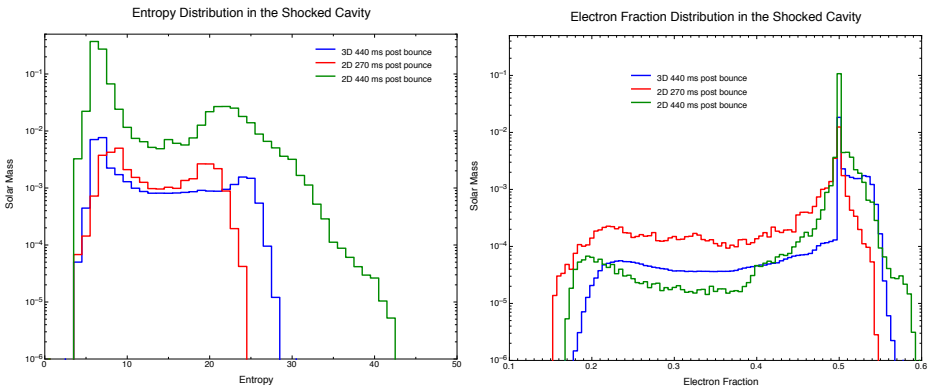

Figure 2: Comparison of the distribution of entropy and electron fraction for two and three dimensional simulations of a 15 msun star from the CHIMERA code.

els. To estimate the mass of ^{56}Ni in the ejecta in the CHIMERA models, all zones with positive local total energy are considered part of the ejecta and the ^{56}Ni masses of these zones are summed. This neglects the effects of later fall back as the shock is decelerated in ejecting the envelope. However, multi-dimensional studies imply that ^{56}Ni is relatively weakly affected by this deceleration [see, e.g., 8, and Sect. 4]. The CHIMERA estimates for ^{56}Ni agree well with observations. This suggests that these models are useful for exploring CCSN nucleosynthesis, despite being axisymmetric.

3. Recent Progress in Three Dimensions

The presence of strong features aligned with the axis of symmetry in these CHIMERA models as well as axisymmetric models from other groups, suggests circumspection in evaluating the reality of two-dimensional simulations, even those that match observational constraints. The ultimate goal is three dimensional simulations, but the computational cost of such simulations is hundreds of times larger than the otherwise equivalent 2D simulations, making extensive surveys of 3D models with the most complete physics currently impracticable. However, individual models are now possible with quite realistic physics. Lentz et al. [9] present preliminary results from otherwise identical 2D and 3D CHIMERA simulations starting from a 15 $M_\odot$ progenitor [5]. Reporting results of the 3D model 440 ms after bounce, we find that an explosion has begun, with the mean shock radius at 740 km. This is significantly delayed in comparison to the companion 2D model, which reaches the same mean shock radius 270 ms after bounce. Similar simulations by Hanke et al. [10] and Takiwaki et al. [11] also highlight the slower development of the explosion in 3D. The differences result, at least in part, from differences in the geometry of accretion and outflow. In contrast to the stable picture in 2D, with persistent polar outflows and equatorial accretion stream, 3D models are much more dynamic, with rising plumes of heated material swaddled by down flowing matter in the interstices, visually reminiscent of solar convection. However, the total accretion rate, as quantified by the mass of the proto-NS, is the same in 2D and 3D until the re-energized shock begins to move outward in the 2D model.

The differences in the geometry, with 3D models remaining quasi-spherical while 2D models develop polar outflows, make the mean radius a less than ideal indicator of the state of the explosion. For example, in the Lentz et al. [9] models, the diagnostic energy of the 3D model 440 ms after bounce is 0.069 Bethe, much larger than the 0.031 Bethe of the companion 2D model at 270 ms after bounce. The more advanced state of the 3D model at this same mean shock radius is also

illustrated in Figure 2, which documents the distributions of entropy and electron fraction (both indicators of the amount of neutrino heating) in both models. These distributions for the 2D model at 440 ms after bounce are also included, by which time the diagnostic energy has reached 0.44 Bethe. Clearly, as the explosions power up, a significant quantity of matter becomes increasingly proton-rich ($Y_e > 0.5$), with the 3D model at 440 ms after bounce significantly more advanced by this measure than the 2D model at 270 ms after bounce despite their similar mean shock radii. The developing explosion is also evident in the amount of matter with high entropy. By this measure too, the 3D model is more advanced than mean shock radius would indicate, with similar amounts of matter at entropies greater than 25 at 440 ms after bounce as the 2D model at 270 ms has matter with entropies larger than 20. Ultimately, it will require realistic 3D simulations reaching times beyond 1 send to establish the similarities between 2D and 3D.

4. The Multi-Dimensional Character of CCSN Nucleosynthesis

The push to go beyond spherically symmetric bomb/piston models is fundamentally driven by observations. Observations of nucleosynthesis in CCSN reveal ejecta that is both geometrically-complex [see, e.g., 12] and elementally-inhomogenous [see, e.g., 13]. The case is particularly persuasive for supernova 1987A. Observed asymmetries in iron lines are most easily explained by the concentration of iron-peak elements into high-velocity "bullets" [14]. The *Bochum event*, the rapid development of fine structure in the H_α line from SN1987A roughly 2 weeks after the explosion [15], was interpreted by Utrobin et al. [16] as an indication that a large ($\sim 10^{-3} M_\odot$) clump of nickel was ejected at high velocity ($\sim$ 4700 km s^{-1}) into the far hemisphere of the supernova. Similarly, near-IR observations of He I lines arising roughly 2 months after explosion were interpreted by Fassia and Meikle [17] as indications of dense clumps of nickel mixed into the hydrogen envelope of SN 1987A. Indications of large-scale but clumpy elemental mixing extend to optical [see, e.g., 18], X-ray [see, e.g., 19] and now γ-ray [see, e.g., 20] observations of supernova remnants. In particular, Grefenstette et al. [20] concluded that the distribution of ^{44}Ti in Cassiopeia A could best be explained by low-mode convective instabilities, rather than spherical explosions even with substantial small scale mixing or bipolar, jet-like explosions. Without doubt, Rayleigh-Taylor instabilities originating at the Si/O and (C+O)/He boundaries induce inhomogeneity [see, e.g., 21, 22], however these instabilities do not mix nickel to sufficiently high velocities to account for observations of Supernova 1987A and other core-collapse supernovae. This implicates the central engine as a source of ejecta inhomogenieties.

Figure 3 illustrates development of aspherical isotopic composition in the axisymmetric 12 $M_\odot$ model from Bruenn et al. [3], whose ejected nickel mass and explosion energy are illustrated in Fig. 1. White points indicate the locations of tracer particles. The current location of the shock can be discerned by the compression and deflection of the radial arrays of these tracers. Neutrino heating has given rise to two strong polar outflows, their composition dominated by ^{56}Ni, punctuated with pockets rich in ^{44}Ti but generally devoid of ^{28}Si, the result of the freezeout from Nuclear Statistical Equilibrium (NSE). In the regions rich in ^{44}Ti, this freezeout is clearly α-rich. Also evident is the remains of the equatorial downflow. Though it's not been fed directly by newly shocked material for nearly a second, part of this cut-off downflow, composed of ^{28}Si and ^{16}O, continues to accrete onto the proto-NS, while the rest is being lifted outward by the neutrino-heated outflows.

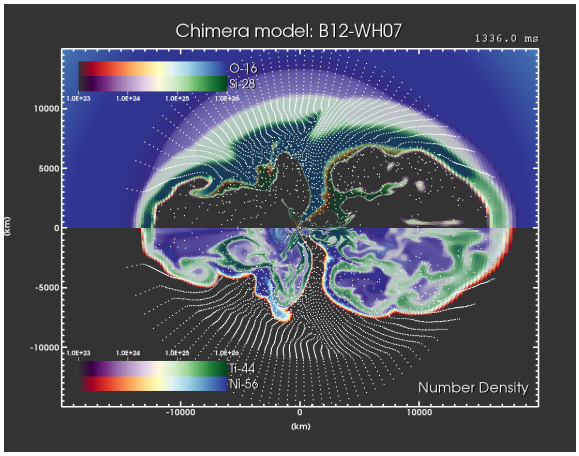

Figure 3: Nucleosynthesis from an axisymmetric simulation of a core-collapse supernovae from a 12 $M_\odot$ star. White dots denote the positions of tracer particles.

Overlying both the downflow and the upflows are the shocked ejecta. In this 12 $M_\odot$ model, once the stalled shock begins its outward progress ($\sim$ 120 ms after bounce), shock burning initially photodisintegrates matter into α-particles and a small quantity of free nucleons. By $\sim$ 300 ms after bounce, the shock has weakened sufficiently that shock silicon burning produces iron group elements. While production of ^{56}Ni and its nuclear neighbors by freezeout is largely complete by 500 ms after bounce, incomplete silicon burning continues to produce some nickel until 600 ms after bounce. Oxygen burning starts as early as 220 ms after bounce in this model as the shock toward the north pole progress into the outer portion of the silicon shell, where ^{16}O represents a small ($\sim$4% by mass) admixture in the composition dominated by ^{28}Si and ^{32}S. In the 12 $M_\odot$ progenitor of Woosley and Heger [5], this O-enriched silicon shell stretches from $\sim$1900–2800 km. Oxygen burning accelerates as more of the shock reaches the O-enriched outer silicon layer. By 290 ms after bounce, the shock in this model first reaches the oxygen layer, where the ^{16}O mass fraction jumps to 78%. The stronger shock along the north pole results in more complete oxygen burning in this direction (contrast the greenish color in this direction at 16,000 km in the upper panel of Fig. 3 with the whiter color in the same layer across lower latitudes). Oxygen burning gradually decelerates between 450 and 800 ms after bounce as the post-shock temperature declines due to the expansion of the shock, causing oxygen burning to become less efficient. From 800 ms after bounce, nuclear transmutations cease to have a significant impact on the composition of the ejecta, however the final details of the composition of the ejecta remain unclear, as final division between ejecta and neutron star remains incomplete [23].

This mass cut is one of the key parameters in bomb/piston models. Often in such models, the placement of the mass cut is motivated by the need to limit neutron-rich ejecta in order to conform to Galactic chemical evolution. Hoffman et al. [24] placed a limit of 10^{-4} $M_\odot$ on the typical amount of neutron-rich ($Y_e < 0.47$) ejecta allowed from each core-collapse supernova, a limit that is easily violated in models without spectral neutrino transport. The mass cut is intimately connected to the accretion rate of matter onto the neutron star. The models of Bruenn et al. [3] demonstrate an accretion rate of material out of the heating region, and ultimately onto the proto-NS, that declines steadily from values of ~ 1 $M_\odot$ s^{-1} as the explosion develops, but levels off at values of ~ 0.01 $M_\odot$ s^{-1} even after the explosion is launched. Even 1.4 seconds after bounce, with the shock beyond 10,000 km, accretion continues at this level, slowly clearing the "Hot Bubble" above the proto-NS.

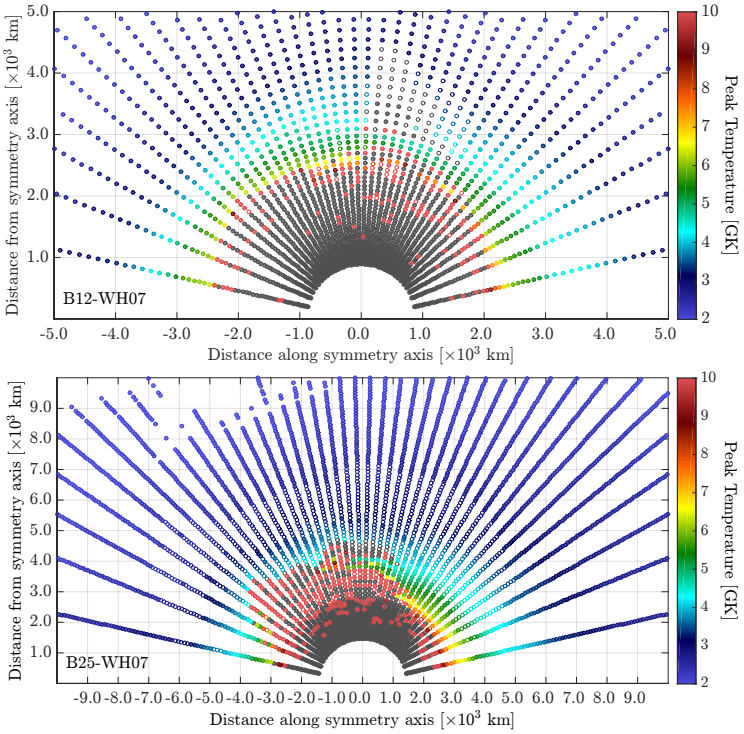

Figure 4: The fate of mass elements in the progenitor for 12 and 25 $M_\odot$ stars. Gray filled circles are matter now in the neutron star, gray open circles represent matter bound to the neutron star. The colored circles are unbound matter, with the color representing the highest temperature reached by the parcel. Filled colored circles have positive radial velocity, open colored circles, though unbound, have negative radial velocity.

Figure 4 uses the tracer particles in CHIMERA to illustrate the mass cut that results from models for 12 and 25 $M_\odot$ stars. Tracers, each representing equal mass, are placed at their initial location in the progenitor, but colored and shaped to reflect their ultimate fate. Tracers colored gray are gravitationally bound to the neutron star (their gravitational potential energy exceeds the sum of their thermal and kinetic energies) while particles of other colors are unbound. The color denotes the maximum temperature experienced by the tracer, which is a reasonable proxy for the composition. For example, the red tracers have all experienced freezeout from NSE while the blue tracers are oxygen-rich matter essentially unaltered from its progenitor composition. Clearly, the mass cut between gray and colored particles is not simply a mass or radial coordinate, with a few tracers escaping from fairly deep layers. Even well above the mass cut, the thickness of the layer of intermediate mass elements (peak temperatures of 4-5 GK) varies considerably with latitude, especially in the 25 $M_\odot$ model. This reflects the varying strength of the shock with latitude in the explosion. The multi-dimensional character of the explosion influences all phases of nucleosynthesis in these models.

The progressive development of the explosion is also evident in Figure 4, which shows the predicted fates of the tracers 1.34 and 1.40 seconds after bounce for the 12 and 25 $M_\odot$ models, respectively. While the fates of the tracers represented by filled circles are relatively certain, with gray filled tracers in the proto-NS and colored filled tracers unbound and headed outward, the fates of tracers marked by open circles are uncertain. Open gray circles are bound to the neutron star, but have not yet accreted onto it, thus they (or some fraction) may still be heated and become unbound. Note the large patch of gray open circles in the 12 $M_\odot$ model near the equator from 3500-4500 km in radius. These are the remnants of the former accretion downflow, still making their way to the

proto-NS. The open colored circles are unbound by the consideration of their total energy (kinetic + thermal - gravitational), but are moving inward, making predictions of their fate, or at least their nucleosynthesis, uncertain. The existence of a significant amount of matter, especially in the 25 $M_{\odot}$ case, whose fate is uncertain even 1.4 seconds after bounce increases the uncertainty in predictions of CCSN nucleosynthesis. Resolving the mass cut in CCSN models, and eventually witnessing the onset of the proto-NS wind (which is being suppressed in these models by ongoing accretion) will require simulations to run much longer than previously considered [23].

References

[1] E. J. Lentz, A. Mezzacappa, O. E. B. Messer, M. Liebendörfer, W. R. Hix, and S. W. Bruenn, ApJ **747**, 73 (2012).

[2] E. J. Lentz, A. Mezzacappa, O. E. B. Messer, W. R. Hix, and S. W. Bruenn, ApJ **760**, 94 (2012).

[3] S. W. Bruenn, E. J. Lentz, W. R. Hix, A. Mezzacappa, J. A. Harris, O. E. B. Messer, E. Endeve, J. M. Blondin, M. A. Chertkow, E. J. Lingerfelt, et al., ApJ **submitted** (2014).

[4] S. W. Bruenn, A. Mezzacappa, W. R. Hix, E. J. Lentz, O. E. Bronson Messer, E. J. Lingerfelt, J. M. Blondin, E. Endeve, P. Marronetti, and K. N. Yakunin, ApJ **767**, L6 (2013).

[5] S. E. Woosley and A. Heger, Phys. Rep. **442**, 269 (2007).

[6] J. J. Eldridge and C. A. Tout, MNRAS **353**, 87 (2004).

[7] S. J. Smartt, J. J. Eldridge, R. M. Crockett, and J. R. Maund, MNRAS **395**, 1409 (2009).

[8] N. J. Hammer, H.-T. Janka, and E. Müller, ApJ **714**, 1371 (2010).

[9] E. J. Lentz, S. W. Bruenn, W. R. Hix, A. Mezzacappa, O. E. B. Messer, E. Endeve, J. M. Blondin, J. A. Harris, P. Marronetti, and K. N. Yakunin, ApJ p. in prep. (2014).

[10] F. Hanke, B. Müller, A. Wongwathanarat, A. Marek, and H.-T. Janka, ApJ **770**, 66 (2013).

[11] T. Takiwaki, K. Kotake, and Y. Suwa, ApJ **786**, 83 (2014).

[12] L. Wang and J. C. Wheeler, ARA&A **46**, 433 (2008).

[13] P. A. Mazzali, K. S. Kawabata, K. Maeda, R. J. Foley, K. Nomoto, J. Deng, T. Suzuki, M. Iye, N. Kashikawa, Y. Ohyama, et al., ApJ **670**, 592 (2007).

[14] J. Spyromilio, W. P. S. Meikle, and D. A. Allen, MNRAS **242**, 669 (1990).

[15] R. W. Hanuschik, G. Thimm, and J. Dachs, MNRAS **234**, 41P (1988).

[16] V. P. Utrobin, N. N. Chugai, and A. A. Andronova, A&A **295**, 129 (1995).

[17] A. Fassia and W. P. S. Meikle, MNRAS **302**, 314 (1999).

[18] W. P. Blair, J. A. Morse, J. C. Raymond, R. P. Kirshner, J. P. Hughes, M. A. Dopita, R. S. Sutherland, K. S. Long, and P. F. Winkler, ApJ **537**, 667 (2000).

[19] J. P. Hughes, C. E. Rakowski, D. N. Burrows, and P. O. Slane, ApJ **528**, L109 (2000).

[20] B. W. Grefenstette, F. A. Harrison, S. E. Boggs, S. P. Reynolds, C. L. Fryer, K. K. Madsen, D. R. Wik, A. Zoglauer, C. I. Ellinger, D. M. Alexander, et al., Nature **506**, 339 (2014).

[21] E. Müller, B. Fryxell, and D. Arnett, A&A **251**, 505 (1991).

[22] M. Herant and W. Benz, ApJ **387**, 294 (1992).

[23] J. A. Harris, W. R. Hix, M. A. Chertkow, S. W. Bruenn, E. J. Lentz, O. E. B. Messer, A. Mezzacappa, J. M. Blondin, P. Marronetti, and K. N. Yakunin, in *Proceedings of Nuclei in the Cosmos XIII*, edited by Z. Elekes, et al. (SISSA Proceedings of Science, 2014), p. 099.

[24] R. D. Hoffman, S. E. Woosley, G. M. Fuller, and B. S. Meyer, ApJ **460**, 478 (1996).